UC Irvine
UC Irvine Previously Published Works

Title

Design of Advanced Thin-Film Catalysts for Electrooxidation of Formic Acid

Permalink

https://escholarship.org/uc/item/02f1s9s5

Journal

ACS Catalysis, 14(4)

ISSN

2155-5435

Authors

Tripković, Dušan V
Milošević, Dragana L
Stevanović, Sanja I
et al.

Publication Date

2024

DOI

10.1021/acscatal.3c05520

Design of Advanced Thin-Film Catalysts for Electrooxidation of Formic Acid

Dušan V. Tripković,* Dragana L. Milošević, Sanja I. Stevanović, Ksenija Dj. Popović, Vladislava M. Jovanović, Pietro P. Lopes, Pedro F B D Martins, Vojislav R. Stamenković, and Dušan Strmčnik

ACCESS | Metrics & More | Article Recommendations | SI Supporting Information

ABSTRACT: Successful development of catalysts for electrochemical formic acid oxidation (FAO) requires finding an optimal balance between catalytic performance (activity, stability, and selectivity) and catalyst cost. While platinum is one of the most active catalyst materials for FAO, it suffers from performance loss at low overpotentials due to poisoning with CO, which is one of the intermediates formed in the so-called indirect path of FAO. In this work, we explored the synergistic effects of the supporting material and annealing temperature on the performance of Pt thin films for FAO in acidic media. Compared to the as-prepared Pt films, the annealed films show up to 5-fold and 15-fold improvement for FAO on Pt@Ni and Pt@Cr, respectively. While the most active Pt@Ni thin film shows the lowest stability, the most active Pt@Cr thin film is also the most stable, challenging conventional trade-offs in electrocatalysis and providing a promising candidate for FAO nanocatalyst synthesis.

**KEYWORDS:** Pt thin films, nickel and chromium, thermal treatment, formic acid, electrooxidation
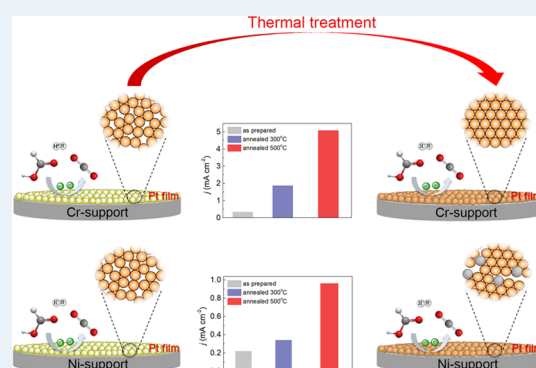
INTRODUCTION

The electrocatalytic oxidation of small organic molecules, such as methanol, ethanol, and formic acid, has been extensively studied due to their properties that make them suitable for use in fuel cells.[1−5] Particularly, the electrochemical oxidation of formic acid has been comprehensively examined as the anodic reaction in a direct formic acid fuel cell (DFAFC) and as a model reaction important for understanding the electro-oxidation of other small organic molecules. On platinum, which is one of the most active metals for formic acid oxidation (FAO), the reaction is known to proceed through a dual-path mechanism. In the direct path, the reaction proceeds directly to CO_2 through an adsorbed intermediate, formate ($HCOO_{ad}$)

$$HCOOH \rightarrow CO_2 + 2H^+ + 2e^- \tag{1}$$
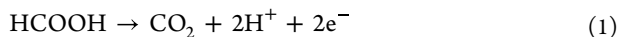
while in the indirect path, the poisoning CO_{ad} species are formed first, before being oxidized to CO_2[6−12]

$$HCOOH \rightarrow COad + H_2O \rightarrow CO_2 + 2H^+ + 2e^- \tag{2}$$
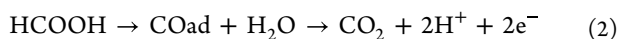
The main goal in the development of the catalysts for FAO is to find the optimal balance between catalytic performance (activity/stability/selectivity) and catalyst cost, i.e., the quantity of the noble metal used.[6,13−15] However, platinum and its alloys, which are among the best catalysts for FAO, are particularly susceptible to poisoning species, which significantly

reduces their catalytic performance at low potentials.[16,17] Several strategies are in place to mitigate this issue, such as tuning the catalyst's selectivity by surface modification with a second metal, tuning its activity by changing the electronic properties via alloying with transition metals, as well as tuning the selectivity/activity through catalyst's surface morphology (facet-dependent catalytic properties).

An additional approach is the tuning of catalyst properties through the introduction of electrochemically stable support material.[18] Interactions between the deposited metal and supports are of crucial importance and can significantly affect the performance of the catalyst. The electronic, geometric, and bifunctional effects originating from strong metal−support interactions (SMSI) can determine the essential catalyst properties, such as activity, selectivity, and stability.[19−22] In conjunction with thermal annealing, this approach also enables the rearrangement of surface atoms and, therefore, can
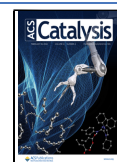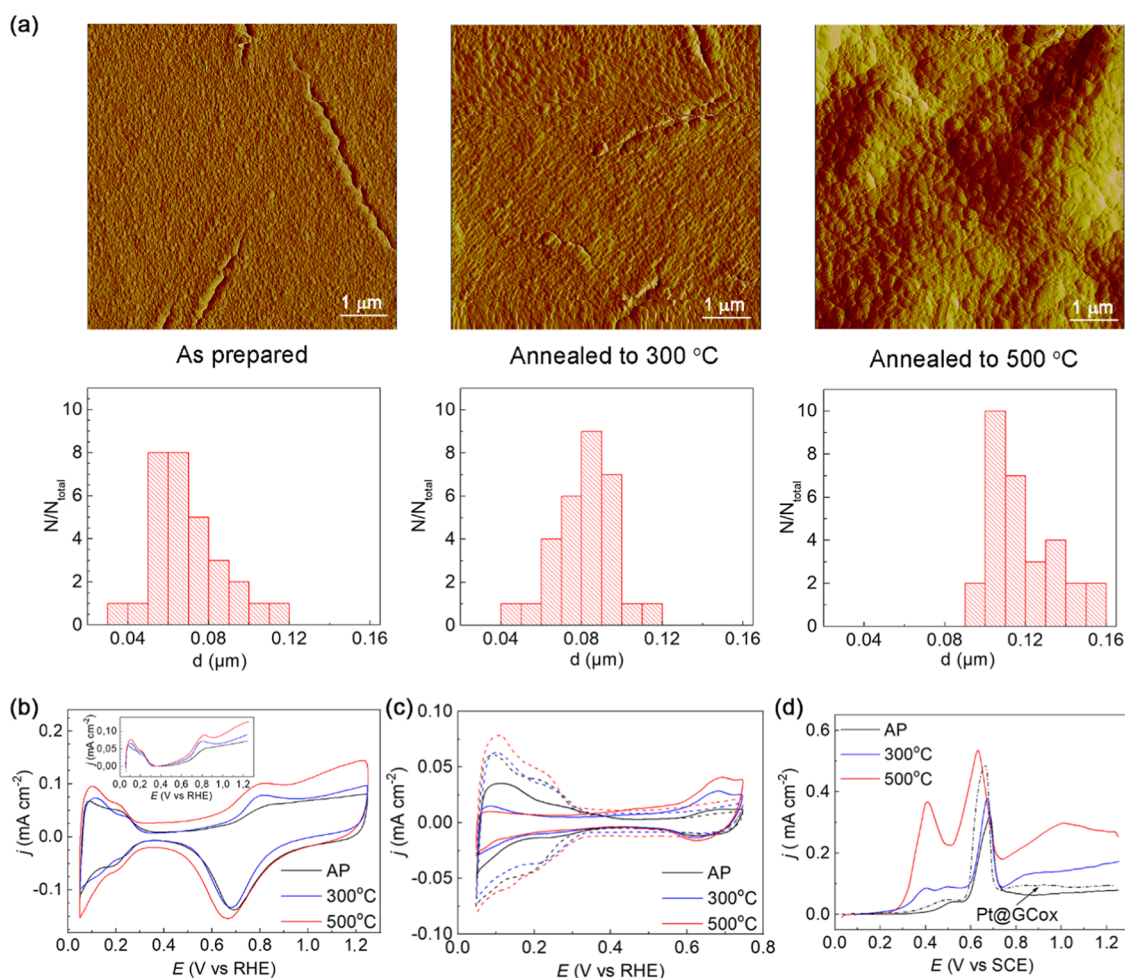
Figure 1. (a) AFM images (5 × 5 μm) and corresponding surface island size distributions for the Pt@Ni catalyst. (b) Voltammograms and positive-going scans after double-layer subtraction (inset) for the Pt@Ni catalyst. (c) Voltammetric profile of the Pt@Ni electrode covered with irreversibly adsorbed bismuth. The dashed line corresponds to the baseline used for the charge measurement. (d) CO stripping curves of the Pt@Ni catalyst (black-dotted line − as-prepared Pt@GCox). Black curves − as-prepared, blue curves − annealed to 300 °C, and red curves − annealed to 500 °C. Test solution: 0.1 M HClO$_4$; sweep rate: 50 mV s^{-1}.

significantly alter the structure of Pt surfaces, including the prospect of alloying with the support.[23,24]

Here, we present a thin-film approach for the design of an advanced electrocatalyst for formic acid oxidation through the utilization of nickel and chromium supports and thermal treatment. In general, among the numerous methods for synthesis, thin-film-based catalysts obtained by deposition of a noble metal over a geometrically defined non-noble metallic substrate serve as a link between well-defined extended single-crystalline surfaces and high-surface-area nanoscale catalysts. Moreover, these systems provide guidelines for real-world catalyst design by effective utilization and transfer of critical physical properties into the catalyst's structure.[25−28] Specifically, for the two different substrates, Ni and Cr, selective combinations of customized electroanalytical methods, thermal annealing in the controlled environment, atomic force microscopy (AFM), and specific adsorption of Bi, including electrooxidation of adsorbed carbon monoxide layer, were used to reveal insights into the structure−function relationship for Pt thin-film catalysts. While annealed Pt@Ni and Pt@Cr show significant improvement, 5-fold and 15-fold, in electrocatalytic activity compared to the as-prepared surfaces, the mechanism of improvement is significantly different. Moreover, the

selectivity and stability of explored surfaces were found to be critically different, with the Pt@Cr annealed surface having the most desirable enhancement of both, which is opposite to commonly observed activity−stability trade-offs in electrocatalysis.[29,30]

■ EXPERIMENTAL SECTION

Electrode Preparation. High-purity Ni and Cr disks (6 mm diameter) were used as the substrate for all thin-film electrodepositions. Before each experiment, Ni and Cr electrodes were mirror polished using silicon carbide grinding paper (Buehler, P800−P4000) and 1−0.05 μm alumina (Buehler). The surface was then rinsed with high-purity water and sonicated for 2−3 min. Before each electrodeposition of platinum, a cyclic voltammogram of a pure Ni or Cr electrode was recorded (potential range 0.05−1.25 V vs RHE and sweep rate 50 mV s^{-1}) in 0.1 M HClO$_4$ solution to ensure that the surface was clean and electrochemically treated.

Platinum was electrochemically deposited on a Ni or Cr substrate under potentiostatic conditions in a deoxygenated 0.1 M HClO$_4$ + 1 mM H$_2$PtCl$_6$ solution. The deposition was carried out in three consecutive steps, from an initial potential hold at 0.05 V vs RHE for 2 s to a final potential of 0.07 V vs
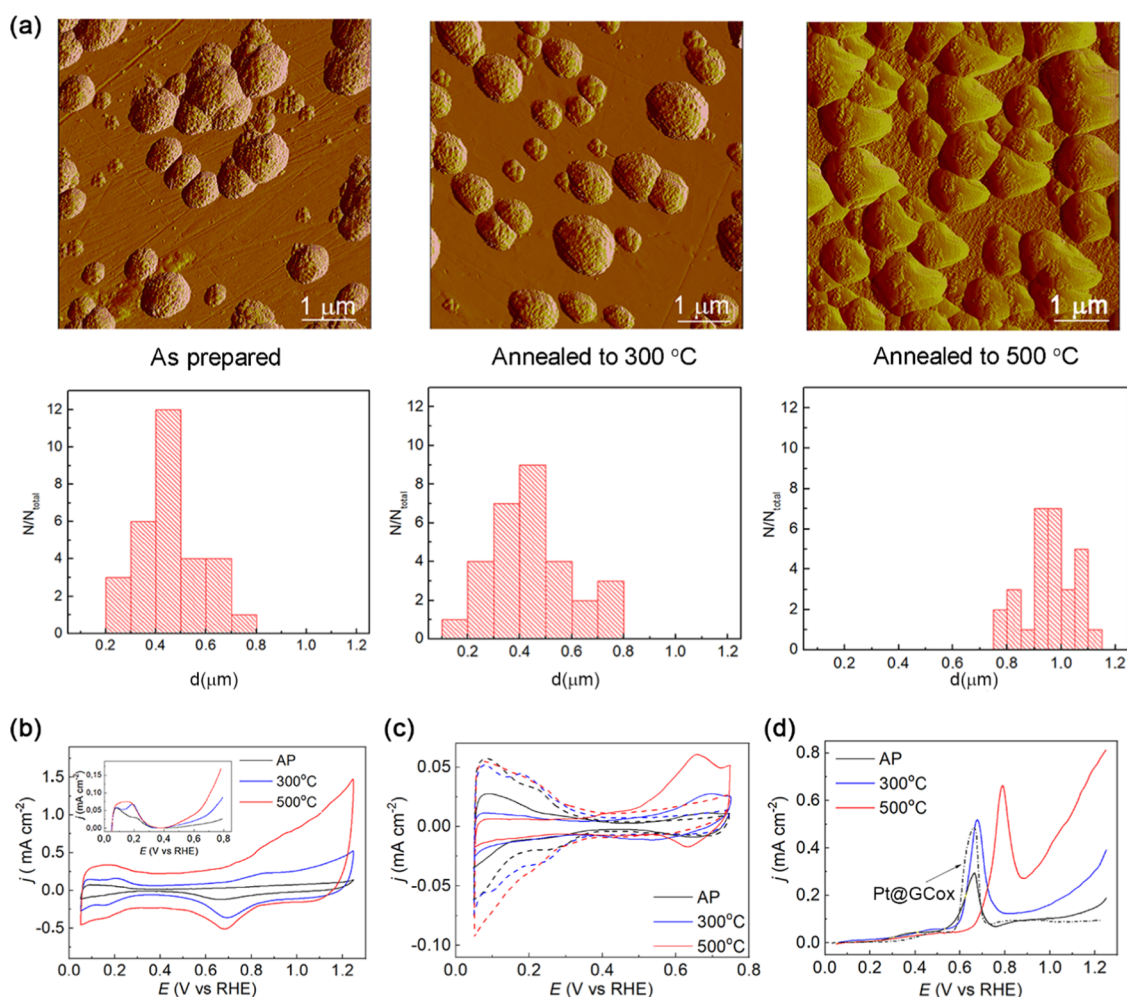
Figure 2. (a) AFM images (5 × 5 μm) and corresponding surface island size distributions for the Pt@Cr catalyst. (b) Voltammograms and positive-going scans after double-layer subtraction (inset) for the Pt@Cr catalyst. (c) Voltammetric profile of the Pt@Cr electrode covered with irreversibly adsorbed bismuth. The dashed line corresponds to the baseline used for the charge measurement. (d) CO stripping curves of the Pt@Cr catalyst (black-dotted line − as-prepared Pt@GC$_{ox}$). Black curves − as-prepared, blue curves − annealed to 300 °C, and red curves − annealed to 500 °C. Test solution: 0.1 M HClO$_4$; sweep rate: 50 mV s^{-1}.

RHE during 50 s. The amount of platinum was estimated from integrated charge measured from the $i−t$ transient response corrected for metal (Ni or Cr, M in further text) substrate charging. This method produces stable Pt thin films with a thickness of around 100 atomic monolayers (MLs), which is approximately 25 nm. After deposition, the as-prepared Pt@M electrode was cycled in the potential between hydrogen and oxygen regions (0.05–1.25 V vs RHE) until a stable voltammogram was reached and then annealed in a reductive atmosphere (95% Ar+5% H$_2$)[31] at a selected temperature, either 300 or 500 °C for 2 h.

Characterization of the Catalysts. Surface characterization of the catalysts was performed at room temperature in air by atomic force microscopy using a NanoScope III D (Veeco) instrument. AFM measurements were carried out in taping mode using silicon nitride cantilevers with a force constant of 0.06 N m^{-1}. Analysis of all surfaces, based on AFM images, was done by selecting 5 different parts of the sample (500 × 500 nm). The measurements of the mean surface island size and size distribution were acquired from a few randomly chosen areas in the AFM images containing about 100 individual islands. AFM measurements were taken before and after thermal treatments.

Electrochemical Measurements. The rotating disk electrode (RDE) measurements were carried out in 0.1 M HClO$_4$ solution at room temperature in a standard three-electrode/three-compartment glass cell. A Pt wire and bridged saturated calomel electrode (SCE) were used as the counter and reference electrodes, respectively. The electrolytes used were prepared with high-purity water ("Millipore," 18.2 MΩ cm resistivity) and p.a. grade chemicals ("Merck"). All solutions were presaturated with nitrogen and kept in an inert atmosphere for the duration of the experiments.

After the deposition of Pt onto the M substrate, the electrodes were thoroughly rinsed with high-purity water and transferred to a cell containing 0.1 M HClO$_4$. The electrochemically active surface area of Pt@M electrodes used was estimated from the integrated charge in the hydrogen adsorption/desorption region (potential range from 0.05 to 0.45 V) and the CO$_{ad}$ stripping curve with a correction for double-layer charging, from the steady-state cyclic voltammograms in the supporting electrolyte, assuming a charge of 210 μC/cm^2 for a monolayer of adsorbed hydrogen and 420 μC/cm^2 for a monolayer of adsorbed CO.

The electrocatalytic activity of Pt@M electrodes for formic acid oxidation was tested in 0.1 M HClO$_4$ solution containing

0.5 M HCOOH ("Merck"), which was added to the supporting electrolyte while the electrode potential was held at 0.05 V. The potential was cycled at a sweep rate of 50 mV s^{-1}. The relevant information on (111) ordered domains on Pt@M samples was obtained from the specific and selective irreversible adsorption of Bi. The detailed procedure was given elsewhere.[32,33]

In Situ FTIR Measurements. All IR measurements were performed in a spectroelectrochemical glass cell designed for an external reflection mode in a thin-layer configuration in 0.1 M HClO$_4$ solution containing 0.5 M HCOOH. The cell is coupled at its bottom with a CaF$_2$ prism beveled at 60° from the prism base. A Nicolet Nexus 670 spectrometer, equipped with a liquid-N$_2$ cooled MCT detector, was used. The spectra were recorded at a resolution of 8 cm^{-1}. All measurements were performed using p-polarized light.

Stability Measurements. To evaluate the stability of Pt@ M against dissolution and deactivation due to potential cycling, a custom-built RDE setup in conjunction with inductively coupled plasma mass spectrometry (ICP-MS) was used. The *in situ* ICP-MS experiments were done using a stationary probe rotating disk electrode (SPRDE) system coupled to an ICP-MS instrument (PerkinElmer) as described elsewhere in the literature.[34] These experiments were carried out in a blank 0.1 M HClO$_4$ electrolyte.

■ RESULTS AND DISCUSSION

Catalyst Surface Characterization. The AFM images of the Pt thin film deposited over Ni and Cr show the difference in morphology (Figures 1a and 2a). This implies that the nature of the substrate can dictate Pt deposition, which results in the different surface morphology. The AFM images of the as-prepared and annealed Ni and Cr substrates are given in the Supporting Information (SI) (Figure S1).

Pt@Ni Surface. Figure 1a shows the surface morphology of differently treated Pt@Ni electrodes revealed by AFM. The As-prepared Pt@Ni electrode consists of predominantly spherical particles with an average size of 60 nm, a fairly uniform distribution, and high-surface coverage. Upon annealing, the particle growth is observed first on Pt@Ni at 300 °C, while at 500 °C, the average particle size becomes approximately 120 nm. In addition, surface roughening can also be observed with the increase of annealing temperature and is the most evident at 500 °C. A close inspection of the cyclic voltammogram for the as-prepared Pt film on the Ni substrate resembles polycrystalline platinum. Consistent with the observed roughening, the voltammograms in Figure 1b exhibit a change in shape in the underpotentially deposited hydrogen (H$_{UPD}$) region (0.05 V < E < 0.4 V) as well as in the region of surface oxide formation (0.45 V < E < 1.25 V).

Apart from the observation that thermal annealing induces a change in the ratio of specific surface structures due to the rearrangement of the surface atoms, it is difficult to discern from the voltammogram alone how annealing affects the ratios of individual crystal planes on the surface. A much better tool to achieve that is the structure-sensitive selective adsorption of Bi (Figure 1c). This method, which was demonstrated to be a convenient surface-specific method for determining the Pt surface structures,[32,33,35] shows an increase of the Pt(111) terrace site fraction from 8% for the as-prepared to 48% for the annealed Pt@Ni at 500 °C (Table 1).

Finally, we note that annealing seems to cause the migration of some Ni from the underlying substrate to the surface. This

Table 1. Fraction of the (111) Ordered Domains Determined for the As-Prepared and Annealed Pt@Ni and Pt@Cr Electrodes

| sample	Pt@Ni	Pt@Cr
as-prepared	8.0%	8.6%
annealed 300 °C	24%	40%
annealed 500 °C	48%	81%

can be concluded from the CO stripping experiments as shown in Figure 1d, where an additional peak can be seen at 0.4 V with the annealing. This peak is usually associated with the oxidation of CO on Ni sites[36,37] and is absent on the as-prepared Pt@Ni surface, which looks very similar to the response obtained on Pt deposited on glassy carbon (Pt@GC) or Cr substrate (Pt@Cr) (Figure 1d). Due to the partial removal of adsorbed CO$_{ad}$ on surface Ni from the annealed Pt@Ni catalyst, the CO stripping peak on Pt is shifted to more negative potentials, in contrast with the expected positive shift due to the increasing fraction of Pt(111) domains in the film.

Pt@Cr Surface. In contrast to the Pt@Ni surface, the as-prepared Pt@Cr electrode (Figure 2a) has predominantly large, spherically shaped Pt islands with a wider size distribution and much lower surface coverage compared to Pt@Ni. With annealing, the islands increase in diameter from an average of 0.45 μm for the as-prepared surface to 1 μm for the annealed surface at 500 °C. Most notably, the islands also change their morphology at higher annealing temperatures (500 °C), becoming more flat and faceted. In the voltammograms (Figure 2b), this is manifested in the H$_{UPD}$ region with an increase of the peak current at 0.3 V, usually associated with (111)x(100) surface sites.[38] At 500 °C, the H$_{UPD}$ area becomes completely flat, resembling a Pt(111) voltammogram. Both Bi adsorption and CO stripping results are also well aligned with this conclusion. The fraction of (111) domains increases from 9% for the as-prepared surface to 81% for the 500 °C annealed surface (Figure 2c and Table 1).

The CO stripping peak in Figure 2d shifts toward more positive potentials with the increase in annealing temperature, which is indicative of restructuring toward the (111) surface, consistent with the trend for the CO stripping peak potential on platinum single: Pt(110) < Pt(100) < Pt(111).[39,40]

After electrochemical and AFM surface structure evaluations, the activity, stability, and selectivity of these catalysts for formic acid oxidation reaction were determined.

Formic Acid Oxidation. The performance of the Pt low-index single crystals was evaluated first in order to establish the basis for understanding the role of surface structure on FOA activity, selectivity, and stability of different surface structures during formic acid oxidation. The characteristic signatures observed for each crystalline structure are given in Figure 3. The dual-path mechanism of the FAO, the direct[41,6] and indirect, both produce CO$_2$ as the final reaction product; nevertheless, they proceed at very different potentials. At low potentials from 0.35 to 0.75 V, which are relevant for formic acid fuel cell operation, the FOA specific activity exhibits the following trend: Pt(111) > Pt(100) > Pt(110), as shown in Figure 3. As abundantly explained in the literature,[9] this trend is based on the selectivity toward the direct reaction pathway, which avoids the formation of poisoning CO$_{ad}$ species. In fact, the simultaneous formation of CO at low potentials on steps and defects is the main cause of the lower activity of Pt(110) and Pt(100) compared to Pt(111). After the removal of CO$_{ad}$
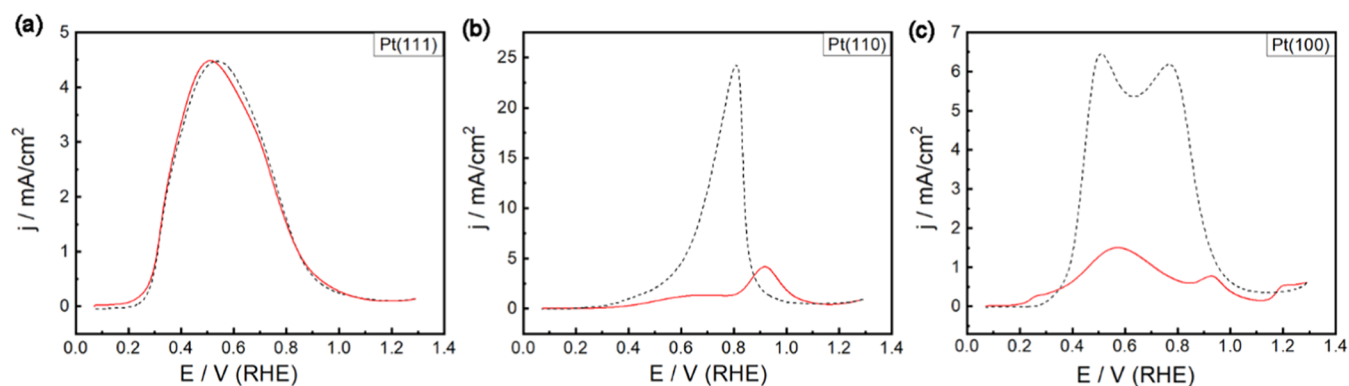
Figure 3. Voltammograms for electrooxidation of 0.5 M HCOOH in 0.1 M HClO$_4$ on (a) Pt(111), (b) Pt(110), and (c) Pt(100) surfaces; positive scan direction, red solid line; negative scan direction, gray dotted line.
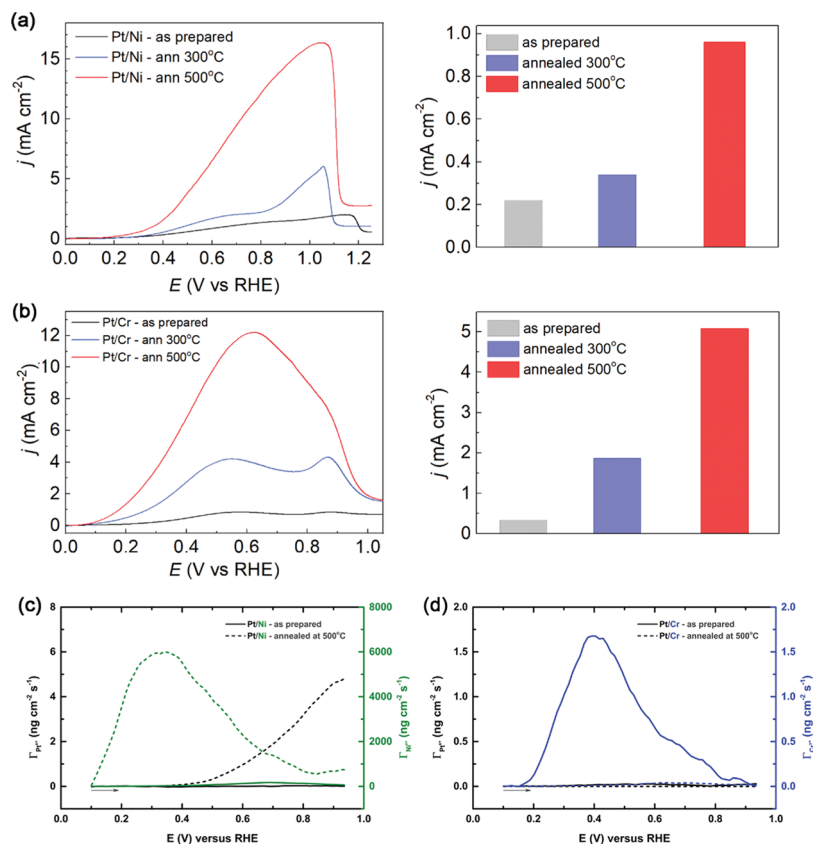
Figure 4. Polarization curves in anodic sweep and corresponding activity obtained at 0.35 V for electrooxidation of 0.5 M HCOOH in 0.1 M HClO$_4$ on (a) Pt@Ni and (b) Pt@Cr surfaces and in situ ICP-MS dissolution of Pt@Ni (c) and Pt@Cr (d) surfaces: as-prepared − solid line; annealed to 500 °C − dashed line.

through electrooxidation, which is facilitated by adsorbed oxygenated species at higher potentials (0.75−1.15 V), the reverse trend of activity occurs: Pt(110) > Pt(100) > Pt(111).[42,43] The height of the oxidation peak in the positive potential region is an indication of the degree of Pt poisoning at lower potentials.[43] Overall, Pt single-crystalline surfaces reveal the cause of structure sensitivity for the catalytic activity of the FAO, which is related to preventing the formation of CO or its removal from the surface through either the direct reaction pathway or the formation of oxygenated surface species, respectively. Finally, we note that these Pt single-crystalline surfaces display negligible dissolution at potentials below 0.5 V.[44]

Next, we analyzed the electrochemical behavior of Pt@Ni and Pt@Cr thin-film catalysts. The polarization curves and corresponding activities at 0.35 V for HCOOH oxidation on differently treated Pt@Ni and Pt@Cr electrodes are summarized in Figure 4.

Note that all voltammograms for the oxidation of formic acid were found to be insensitive to the rotation of the electrode, indicating that the reaction is still under kinetic control within the entire potential region. Anodic and cathodic scans are given in the SI (Figure S2).

The voltammogram of the as-prepared Pt@Ni electrode (Figure 4a) shows distinct similarities with the Pt (110) surface, typical for polycrystalline samples, with two broad

peaks/plateaus centered between 0.25 and 0.85 and 0.85−1.15 V. Upon annealing, both peaks show a substantial increase in current density as well as a shift toward negative potential, reaching the maximum activity at 500 °C. Compared to the as-prepared surface, or Pt (110), the activation at 0.35 V is roughly 5-fold. However, the effect seems to be much more pronounced on the more positive peak, which dominates the overall electrochemical response. The observed activation for the FAO, based on the CO stripping experiments, is attributed to the effect of Ni present on the surface. With the improved ability of the surface to remove the adsorbed CO formed during FAO, the Pt@Ni surface is becoming more active for the indirect reaction path. It should be mentioned that the increased presence of (111) sites, determined by the Bi_{UPD} method, can also contribute to the activity increase via a direct path. Nevertheless, the relative fraction of 48% is not enough to sustain the activity at low potentials without the assistance of CO removal by oxygenated species.

Similar to the Pt@Ni surface, the voltammogram of the as-prepared Pt@Cr electrode (Figure 4b-black curve) resembles that of Pt (110), with the reaction proceeding through both paths presented by two anodic peaks of almost equal activity. However, the changes after annealing the Pt@Cr electrode to 300 and 500 °C are quite different from those in the case of Pt@Ni. In contrast to the Pt@Ni electrode, the first process, associated with the direct path, is prevalent, resulting in a bell-shaped curve, which is typical for a Pt(111) single-crystal electrode (Figure 3a). The specific activity increase is almost 15-fold compared to the as-prepared surface and 2-fold compared to Pt (111). We attribute such activity boost to the thermal treatment-induced surface reconstruction in favor of (111) orientation and full segregation of Pt over Cr. This is in good agreement with the observations obtained by AFM, voltammetry, and Bi_{UPD}, which confirmed a dramatic increase in the fraction of Pt (111) facets. Nevertheless, it was important to confirm that the FAO was indeed proceeding through the direct oxidation of HCOOH to CO_2, without significant formation of the CO_{ad} poisoning species. In situ FTIR analysis has revealed that the Pt@Cr surface annealed at 500 °C (Supporting Information Figure S3 3d) does not have a CO_{ad} peak at any potential during the electrooxidation of formic acid, which implies that the reaction proceeds without the formation of CO_{ad}, i.e., the same way as on Pt(111) (Supporting Information Figure S3 (3b)). These results confirm a significant activity increase on both substrates upon annealing as well as the selectivity increase toward the direct FOA mechanism on Pt@Cr.

To complete the performance characterization of our supported thin films, we performed stability testing of annealed and as-prepared surfaces during FAO by SPRDE-ICP-MS. The Pt-like stability of the as-prepared Pt@Ni surface, with essentially no dissolution of Pt or Ni at potentials below 0.75 V vs RHE (Figure 4c), suggests that the deposited Pt film on Ni is dense and nonporous. Upon annealing, which significantly increases the activity of the surface, a massive dissolution of both Pt and Ni was detected already at potentials around −0.35 V. Again, the explanation for the observed effect is indicated by the CO stripping experiments (Figure 1d), which show that a substantial amount of Ni seems to migrate to the surface upon annealing, causing an extensive dissolution of Ni in the acidic environment as well as making the adjacent Pt more prone to degradation. This is in line with the so-called inverse activity−stability relationship, which postulates that

there is a trade-off between the activity and stability of electrocatalytic materials. In rare examples, however, an inverse of this relationship is observed. We found that our annealed Pt@Cr system falls into that category. The as-prepared Pt@Cr catalyst shows signs of significant dissolution of the Cr substrate, while the Pt film is stable at potentials below 0.75 V vs RHE, which is a direct consequence of the island-like film morphology, leaving substantial portions of the Cr exposed. Interestingly, annealing of the Pt@Cr sample caused, in addition to the 15-fold activation at 0.15 V RHE, 2 orders of magnitude lower dissolution of Cr at the same potential as well as additional stabilization of the Pt film. We attribute the stabilization of Pt to a higher fraction of the inherently more stable (111) facets in the annealed sample, while the origin of the Cr stability seems to be some sort of passivation during annealing, most likely by trace oxygen in the annealing gas (SI, Figure S4). Nonetheless, the 500 °C annealed Pt@Cr catalyst was found to be the most active, selective, and stable catalyst in our study. A catalyst with the best marks for all three characteristics is a very rare find in electrocatalysis in general.

■ CONCLUSIONS

In the work presented, we explored the synergistic effects of the supporting material and annealing temperature on the performance of Pt thin-film catalysts for formic acid electro-oxidation in acidic media. Our results show that compared to the as-prepared Pt films, the annealed (500 °C) Pt@Ni and Pt@Cr films show exceptional activity for the FAO reaction, with 5-fold and 15-fold improvement, respectively.

On annealed Pt@Ni, the activation is a consequence of the bifunctional effect, i.e., formic acid is oxidized predominantly on platinum through the indirect pathway forming CO in the process, while the poisoning CO_{ad} is oxidized on adjacent Ni, which has migrated to the surface during annealing, resulting in improved activity. However, the increase in activity leads to enhanced instability of the thin-film catalyst, and a significant dissolution of both Pt and Ni is observed in the relevant potential window, in line with the often-observed activity−stability relationship.

In contrast, the improved activity on the annealed Pt@Cr system is a consequence of the surface reconstruction of the Pt film with a predominant (111) orientation. Compared to other facets, the (111) facet selectively favors direct HCOOH oxidation, avoiding CO_{ad} poisoning and thus higher activity at low potentials. Moreover, the Pt (111) facets offer improved stability of the catalyst compared to that of the as-prepared polycrystalline film. Finally, the Cr substrate also experiences improved stability after annealing, presumably due to the formation of a protective oxide layer. Thus, with the successful choice of the supporting material and annealing temperature, we were able to create a thin-film catalyst with improved activity, selectivity, and stability, which is quite rare in electrocatalysis.

■ ASSOCIATED CONTENT

ⓢ Supporting Information

The Supporting Information is available free of charge at https://pubs.acs.org/doi/10.1021/acscatal.3c05520.

> Figure S1. AFM images (5x5 microns) for pure (a) Ni and (b) Cr: as prepared, annealed to 300 °C and annealed to 500 °C; Figure S2. voltammograms for electrooxidation of 0.5 M HCOOH in 0.1 M $HClO_4$ on;

Figure S3. CO_{ad} peaks obtained from in situ FTIR at 0.53V for electrooxidation of 0.5 M HCOOH in 0.1 M $HClO_4$; Figure S4. XPS spectra for Pt@Ni and Pt@Cr before and after annealing (PDF)

■ AUTHOR INFORMATION

Corresponding Author

Dušan V. Tripković − *University of Belgrade - Institute of Chemistry, Technology and Metallurgy, Department of Electrochemistry, 11000 Belgrade, Serbia;* orcid.org/0009-0008-9490-2473; Email: dusan@ihtm.bg.ac.rs

Authors

Dragana L. Milošević − *University of Belgrade - Institute of Chemistry, Technology and Metallurgy, Department of Ecology and TechnoEconomics, 11000 Belgrade, Serbia*

Sanja I. Stevanović − *University of Belgrade - Institute of Chemistry, Technology and Metallurgy, Department of Electrochemistry, 11000 Belgrade, Serbia;* orcid.org/0000-0003-2157-5754

Ksenija Dj. Popović − *University of Belgrade - Institute of Chemistry, Technology and Metallurgy, Department of Electrochemistry, 11000 Belgrade, Serbia*

Vladislava M. Jovanović − *University of Belgrade - Institute of Chemistry, Technology and Metallurgy, Department of Electrochemistry, 11000 Belgrade, Serbia*

Pietro P. Lopes − *Materials Science Department, Argonne National Laboratory, ZIP 60439 Lemont, Illinois, United States;* orcid.org/0000-0003-3211-470X

Pedro F B D Martins − *University of Ljubljana, Faculty of Chemistry and Chemical Technology, SI-1000 Ljubljana, Slovenia; National Institute of Chemistry, SI-1000 Ljubljana, Slovenia;* orcid.org/0000-0002-7078-0378

Vojislav R. Stamenković − *Department of Chemical and Biomolecular Engineering, Horiba Institute for Mobility and Connectivity University of California Irvine, Irvine, California 92697-2700, United States;* orcid.org/0000-0002-1149-3563

Dušan Strmčnik − *National Institute of Chemistry, SI-1000 Ljubljana, Slovenia;* orcid.org/0000-0002-3021-2771

Complete contact information is available at:
https://pubs.acs.org/10.1021/acscatal.3c05520

Author Contributions

D.V.T. conceptualized this work, wrote the original manuscript draft, and performed in-depth data analysis. D.L.M. drew the visualizations and performed image editing. S.I.S. performed the AFM measurements. K.D.P. carried out the Bi adsorption experiments and manuscript draft revision. V.M.J. carried out the manuscript revision. P.P.L. and P.F.B.D.M. carried out the ICP-MS measurements. V.R.S. performed the final review and editing of the manuscript. D.S. analyzed the data and cowrote the paper.

Notes

The authors declare no competing financial interest.

■ ACKNOWLEDGMENTS

■ REFERENCES

(1) Parsons, R.; VanderNoot, T. The Oxidation of Small Organic Molecules. A Survey of Recent Fuel Cell Related Research. *J. Electroanal. Chem.* **1988**, *257* (1−2), 9−45.

(2) Jarvi, T.; Stuve, E. Fundamental Aspects of Vacuum and Electrocatalytic Reactions of Methanol and Formic Acid on Platinum Surfaces. *Electrocatalysis* **1998**, 75.

(3) Reitz, W. Handbook of Fuel Cells: Fundamentals, Technology, and Applications, (Volume 2) W. Vielstich, A. Lamm, and H. A. Gasteiger (Editors). *Mater. Manuf. Processes* **2007**, *22* (6), 789.

(4) Markovic, N.; Ross, P. N. Surface Science Studies of Model Fuel Cell Electrocatalysts. *Surf. Sci. Rep.* **2002**, *45* (4−6), 117−229.

(5) Jiang, K.; Zhang, H. X.; Zou, S.; Cai, W. Bin. Electrocatalysis of Formic Acid on Palladium and Platinum Surfaces: From Fundamental Mechanisms to Fuel Cell Applications. *Phys. Chem. Chem. Phys.* **2014**, *16* (38), 20360−20376.

(6) Capon, A.; Parsons, R. The Oxidation of Formic Acid at Noble Metal Electrodes Part III. Intermediates and Mechanism on Platinum Electrodes. *J. Electroanal. Chem.* **1973**, *45* (2), 205−231.

(7) Iwasita, T.; Xia, X.; Herrero, E.; Liess, H. D. Early Stages during the Oxidation of HCOOH on Single-Crystal Pt Electrodes as Characterized by Infrared Spectroscopy. *Langmuir* **1996**, *12* (17), 4260−4265.

(8) Herrero, E.; Feliu, J. M. Understanding Formic Acid Oxidation Mechanism on Platinum Single Crystal Electrodes. *Curr. Opin. Electrochem.* **2018**, *9*, 145−150.

(9) Boronat-González, A.; Herrero, E.; Feliu, J. M. Heterogeneous Electrocatalysis of Formic Acid Oxidation on Platinum Single Crystal Electrodes. *Curr. Opin. Electrochem.* **2017**, *4* (1), 26−31.

(10) Cuesta, A.; Cabello, G.; Osawa, M.; Gutiérrez, C. Mechanism of the Electrocatalytic Oxidation of Formic Acid on Metals. *ACS Catal.* **2012**, *2* (5), 728−738.

(11) Ferre-Vilaplana, A.; Perales-Rondón, J. V.; Buso-Rogero, C.; Feliu, J. M.; Herrero, E. Formic Acid Oxidation on Platinum Electrodes: A Detailed Mechanism Supported by Experiments and Calculations on Well-Defined Surfaces. *J. Mater. Chem. A* **2017**, *5* (41), 21773−21784.

(12) Xu, J.; Yuan, D.; Yang, F.; Mei, D.; Zhang, Z.; Chen, Y. X. On the Mechanism of the Direct Pathway for Formic Acid Oxidation at a Pt(111) Electrode. *Phys. Chem. Chem. Phys.* **2013**, *15* (12), 4367−4376.

(13) Rice, C.; Ha, S.; Masel, R. I.; Wieckowski, A. Catalysts for Direct Formic Acid Fuel Cells. *J. Power Sources* **2003**, *115* (2), 229−235.

(14) Yu, X.; Pickup, P. G. Recent Advances in Direct Formic Acid Fuel Cells (DFAFC). *J. Power Sources* **2008**, *182* (1), 124−132.

(15) Jiang, J.; Kucernak, A. Nanostructured Platinum as an Electrocatalyst for the Electrooxidation of Formic Acid. *J. Electroanal. Chem.* **2002**, *520* (1−2), 64−70.

(16) Park, S.; Xie, Y.; Weaver, M. J. Electrocatalytic Pathways on Carbon-Supported Platinum Nanoparticles: Comparison of Particle-Size-Dependent Rates of Methanol, Formic Acid, and Formaldehyde Electrooxidation. *Langmuir* **2002**, *18* (15), 5792−5798.

(17) Wang, X.; Hu, J. M.; Hsing, I. M. Electrochemical Investigation of Formic Acid Electro-Oxidation and Its Crossover through a Nafion Membrane. *J. Electroanal. Chem.* **2004**, *562* (1), 73−80.

(18) Samjeské, G.; Miki, A.; Ye, S.; Osawa, M. Mechanistic Study of Electrocatalytic Oxidation of Formic Acid at Platinum in Acidic Solution by Time-Resolved Surface-Enhanced Infrared Absorption Spectroscopy. *J. Phys. Chem. B* **2006**, *110* (33), 16559−16566.

(19) Wang, Y. J.; Wilkinson, D. P.; Zhang, J. Noncarbon Support Materials for Polymer Electrolyte Membrane Fuel Cell Electrocatalysts. *Chem. Rev.* **2011**, *111* (12), 7625−7651.

(20) Maillard, F.; Bonnefont, A.; Micoud, F. An EC-FTIR Study on the Catalytic Role of Pt in Carbon Corrosion. *Electrochem. Commun.* **2011**, *13* (10), 1109−1111.

(21) Cerri, I.; Nagami, T.; Davies, J.; Mormiche, C.; Vecoven, A.; Hayden, B. Innovative Catalyst Supports to Address Fuel Cell Stack Durability. *Int. J. Hydrogen Energy* **2013**, *38* (1), 640−645.

(22) Fu, Q.; Wagner, T. Interaction of Nanostructured Metal Overlayers with Oxide Surfaces. *Surf. Sci. Rep.* **2007**, *62* (11), 431−498.

(23) Pan, C. J.; Tsai, M. C.; Su, W. N.; Rick, J.; Akalework, N. G.; Agegnehu, A. K.; Cheng, S. Y.; Hwang, B. J. Tuning/Exploiting Strong Metal-Support Interaction (SMSI) in Heterogeneous Catalysis. *J. Taiwan Inst. Chem. Eng.* **2017**, *74*, 154−186.

(24) Su, Y.; Feng, M.; Liu, H.; Zhang, C.; Yan, Z.; Yan, Z.; Feng, M.; Liu, H.; Tang, J.; Tang, J.; Du, H. Platinum Nanowires: Structural and Catalytic Evolution upon Annealing Temperature. *Electrochim. Acta* **2015**, *164*, 182−186.

(25) Chung, D. Y.; Chung, Y. H.; Jung, N.; Choi, K. H.; Sung, Y. E. Correlation between Platinum Nanoparticle Surface Rearrangement Induced by Heat Treatment and Activity for an Oxygen Reduction Reaction. *Phys. Chem. Chem. Phys.* **2013**, *15* (32), 13658−13663.

(26) Snyder, J.; Danilovic, N.; Paulikas, A. P.; Tripkovic, D.; Strmcnik, D.; Markovic, N. M.; Stamenkovic, V. R. Thin Film Approach to Single Crystalline Electrochemistry. *J. Phys. Chem. C* **2013**, *117* (45), 23790−23796.

(27) Snyder, J.; Markovic, N. M.; Stamenkovic, V. R. Single Crystalline Thin Films as a Novel Class of Electrocatalysts. *J. Serb. Chem. Soc.* **2013**, *78* (11), 1689−1702.

(28) Van Der Vliet, D. F.; Wang, C.; Tripkovic, D.; Strmcnik, D.; Zhang, X. F.; Debe, M. K.; Atanasoski, R. T.; Markovic, N. M.; Stamenkovic, V. R. Mesostructured Thin Films as Electrocatalysts with Tunable Composition and Surface Morphology. *Nat. Mater.* **2012**, *11* (12), 1051−1058.

(29) Beermann, V.; Gocyla, M.; Kühl, S.; Padgett, E.; Schmies, H.; Goerlin, M.; Erini, N.; Shviro, M.; Heggen, M.; Dunin-Borkowski, R. E.; Muller, D. A.; Strasser, P. Tuning the Electrocatalytic Oxygen Reduction Reaction Activity and Stability of Shape-Controlled Pt-Ni Nanoparticles by Thermal Annealing -Elucidating the Surface Atomic Structural and Compositional Changes. *J. Am. Chem. Soc.* **2017**, *139* (46), 16536−16547.

(30) Hanief, N.; Lang, C. I.; Bucher, R.; Topic, M. Phase Transformations and Surface Characterization of the Platinumchromium Coated System. *J. South. Afr. Inst. Min. Metall.* **2012**, *112* (7), 501−504.

(31) Tripković, D.; Popović, K. D.; Jovanović, V. M.; Nogueira, J. A.; Varela, H.; Lopes, P. P.; Strmcnik, D.; Stamenkovic, V. R.; Markovic, N. M. Tuning of Catalytic Properties for Electrooxidation of Small Organic Molecules on Pt-Based Thin Films via Controlled Thermal Treatment. *J. Catal.* **2019**, *371*, 96−105.

(32) Clavilier, J.; Feliu, J. M.; Aldaz, A. An Irreversible Struci'ure Sensitive Adsorption Bismuth Undeizpotential Deposition at Platinum Electrodes. *J. Electroanal. Chem. Interfacial Electrochem.* **1988**, *243*, 419−433.

(33) Rodríguez, P.; Herrero, E.; Solla-Gullón, J.; Vidal-Iglesias, F. J.; Aldaz, A.; Feliu, J. M. Specific Surface Reactions for Identification of Platinum Surface Domains: Surface Characterization and Electrocatalytic Tests. *Electrochim. Acta* **2005**, *50* (21), 4308−4317.

(34) Lopes, P. P.; Strmcnik, D.; Tripkovic, D.; Connell, J. G.; Stamenkovic, V.; Markovic, N. M. Relationships between Atomic Level Surface Structure and Stability/Activity of Platinum Surface Atoms in Aqueous Environments. *ACS Catal.* **2016**, *6* (4), 2536−2544.

(35) Devivaraprasad, R.; Kar, T.; Chakraborty, A.; Singh, R. K.; Neergat, M. Reconstruction and Dissolution of Shape-Controlled Pt Nanoparticles in Acidic Electrolytes. *Phys. Chem. Chem. Phys.* **2016**, *18* (16), 11220−11232.

(36) Chen, Y.; Shi, J.; Chen, S. Small Molecule (CO, H2) Electro Oxidation as an Electrochemical Tool for Characterization of Ni@Pt/C with Different Pt Coverages. *J. Phys. Chem. C* **2015**, *119* (13), 7138−7145.

(37) Chung, Y. H.; Chung, D. Y.; Jung, N.; Park, H. Y.; Yoo, S. J.; Jang, J. H.; Sung, Y. E. Origin of the Enhanced Electrocatalysis for Thermally Controlled Nanostructure of Bimetallic Nanoparticles. *J. Phys. Chem. C* **2014**, *118* (19), 9939−9945.

(38) Koper, M. T. M. Structure Sensitivity and Nanoscale Effects in Electrocatalysis. *Nanoscale* **2011**, *3* (5), 2054−2073.

(39) García, G.; Koper, M. T. M. Stripping Voltammetry of Carbon Monoxide Oxidation on Stepped Platinum Single-Crystal Electrodes in Alkaline Solution. *Phys. Chem. Chem. Phys.* **2008**, *10* (25), 3802−3811.

(40) Yang, Y.; Agarwal, R. G.; Hutchison, P.; Rizo, R.; Soudackov, A. V.; Lu, X.; Herrero, E.; Feliu, J. M.; Hammes-Schiffer, S.; Mayer, J. M.; Abruña, H. D. Inverse Kinetic Isotope Effects in the Oxygen Reduction Reaction at Platinum Single Crystals. *Nat. Chem.* **2023**, *15* (2), 271−277.

(41) Cuesta, A.; Cabello, G.; Gutiérrez, C.; Osawa, M. Adsorbed Formate: The Key Intermediate in the Oxidation of Formic Acid on Platinum Electrodes. *Phys. Chem. Chem. Phys.* **2011**, *13* (45), 20091−20095.

(42) Adžić, R.; Tripković, A. V.; Vesšović, V. B. Structural Effects in Electrocatalysis: Oxidation of Formic Acid and Hydrogen Adsorption on Platinum Single-Crystal Stepped Surfaces. *J. Electroanal. Chem.* **1986**, *204* (1−2), 329−341.

(43) Grozovski, V.; Climent, V.; Herrero, E.; Feliu, J. M. Intrinsic Activity and Poisoning Rate for HCOOH Oxidation on Platinum Stepped Surfaces. *Phys. Chem. Chem. Phys.* **2010**, *12* (31), 8822−8831.

(44) Lopes, P. P.; Li, D.; Lv, H.; Wang, C.; Tripkovic, D.; Zhu, Y.; Schimmenti, R.; Daimon, H.; Kang, Y.; Snyder, J.; Becknell, N.; More, K. L.; Strmcnik, D.; Markovic, N. M.; Mavrikakis, M.; Stamenkovic, V. R. Eliminating Dissolution of Platinum-Based Electrocatalysts at the Atomic Scale. *Nat. Mater.* **2020**, *19* (11), 1207−1214.